INTERNATIONAL JOURNAL OF HEAT AND TECHNOLOGY

ISSN: 0392-8764
Vol. 34, No. 4, December 2016, pp. 677-686
DOI: 10.18280/ijht.340418

A publication of IIETA

IIETA International Information and Engineering Technology Association
Advancing the World of Information and Engineering

http://www.iieta.org/Journals/IJHT

On High-Strength Low-Shrinkage Iots-Based Concrete

Biyao Geng[1,2,5,6], Wen Ni[1,2*], Hui Wu[3], Xiaoyan Huang[1,2], Xiaowei Cui[1,2,4], Shuang Wang[1,2] and Siqi Zhang[1,2]

[1]Key Laboratory of the Ministry of Education of China for High-Efficient Mining and Safety of Metal Mines, School of Civil and Environmental Engineering, University of Science and Technology Beijing, Beijing 100083, China
[2]Beijing Key Laboratory on Resource-oriented Treatment of Industrial Pollutants, Beijing 100083, China
[3]Material & Engineering Examination Dept. the Patent Office of the State Intellectual Property Office of the People's Republic of China; Beijing 100088, China
[4]Shangluo College, Chemistry and Chemical Engineering, Shangluo Shanxi, 726000, China
[5]Beijing Weitong Environment Technology co., ltd., Beijing, China
[6]Beijing Yujin Resources and Environment Technology Institute, 101502, Beijing, China

Email: niwen@ces.ustb.edu.cn

ABSTRACT

With iron ore tailings (IOTs) as the main raw material, the author prepares concrete specimens featuring low shrinkage and high bending strength, and reduces the shrinkage with "hot steaming" steel slag as the admixture. Then, the author carries out a series of laboratory tests to characterize the shrinkage, strength, morphology, microstructure and chemical components of the specimens during the curing process. These parameters are measured after 12 hours, 3 days, 7 days and 28 days, respectively. For each mixture, 3 replicates are prepared and analyzed by the strength test, X-Ray diffraction (XRD), Fourier transform infrared spectroscopy (FTIR), and scanning electron microscope (SEM). The measured shrinkage of the proposed concrete is lower than half of that of the normal concrete for railway sleepers, and its bending strength is almost twice of that of the latter. Further investigation demonstrates that the large decrease in the autogenous shrinkage is attributable to the micro-expansion, which is caused by the hydration of f-CaO, f-MgO and RO phases in the highly dispersed steel slag particles. In the early stage of curing, the shrinkage might be mitigated by the coordinated formation of ettringite and C-S-H gels. Besides, the reduced shrinkage leads to fewer stress loss of prestressed reinforcement in prefabricated structures. The findings indicate that the proposed concrete has a great potential to serve as the material for prefabricated structures or cast-in-situ concretes.

Keywords: Low shrinkage, Iron ore tailings, Steel slag, Ettringite, High bending strength.

1. INTRODUCTION

With rapid development in concrete structure construction, China consumes more than 5 billion tons of aggregates each year. Most of the aggregates are excavated from limestone deposits. Blasting excavation alone consumes over 1 million tons of explosives. Whereas trinitrotoluene (TNT) and other mainstream explosives are composed of more than 50% nitryl by weight, the blasting excavation produces a vast amount of NO_x. Moreover, the blasting of every cubic meter of rocks results in 0.027~ 0.17 kg dust less than 1.4 microns in diameter [1]. It is estimated that the fine particle matters (PM2.5) produced blasting excavation of limestone is almost equivalent to that emitted by automobiles in China. Therefore, it is necessary to find alternative materials for concrete aggregates. The possible options include is ore tailings and steel slag.

China has a gigantic store of ore tailings, which mainly come from the ore beneficiation process. By the end of 2013, the country has over 16 billion tons of ore tailings, one-third of which is iron ore tailings (IOTs) [2]. To make matters worse, the amount is still increasing by over 1 billion tons per year [3]. The huge amount of ore tailings not only leads to high land occupation, severe environmental pollution and ecological damages, but also brings imminent threat to personal safety in regions where tailing dams are overused. As a result, it is an urgent issue to find a way to recycle and reuse the tailings [4]. Recently, a new type of high performance concrete has attracted many attentions because IOTs constitutes 70% of its raw materials [5-6]. This type of

concrete can serve as material of prefabricated structurals or cast-in-situ concrete.

As above, it is a better strategy to produce concrete mainly made of IOTs than to make concrete aggregates from limestone. During the curing process, however, shrinkage is a big concern for the new type of concrete as it features very low water cement ratio and no coarse aggregate.

Many literatures [7-8] claim that, concrete with a very low water cement ratio would shrink substantially during the curing process, even if the humidity outdoor is desirable. The primary cause of the shrinkage lies in the low permeability, i.e. the amount of water seeping into the concrete is greatly limited. Under the effect of hydration, self-desiccation shrinkage would occur, which in turn leads to partial autogenous shrinkage [9-10]. Moreover, the autogenous shrinkage of this type of concrete may also induce a substantial stress loss of prestressed reinforcement, which hinders the application of the concrete in engineering practices.

Similar to ore tailings, steel slag is a major industrial waste in China. Only a small part of steel slag is rich in metal iron, which can be extracted and recycled. [9-11] For most of steel slag, there is no solution for comprehensive utilization. For centuries, researchers have tried to turn steel slag into building materials. However, the attempts mostly end up in failure because of the overexpansion effect. Steel slag tends to expand because of the high content of well crystallized free-CaO (f-CaO), free-MgO (f-MgO) and solid solution phases of MgO, FeO and CaO (RO phases) [11-12]. Fortunately, there is a new steel slag pretreatment technology, known as “hot steaming” that can convert most of the free MgO and CaO in the slag into corresponding hydroxides [13], which mitigate and put slag expansion under control in most of the circumstances. This pretreatment technology creates a promising future for producing building materials with steel slag as the raw material.

Recognizing the shortcomings of existing high strength concrete, the author decides to develop a type of high performance concrete featuring both low shrinkage and high bending strength. In this paper, steel slag is introduced to the IOTs-based high strength concrete of railway sleepers, aiming at minimizing the autogenous shrinkage and improving the potential of the concrete to serve as materials of prestressed structures or as cast-in-situ concrete. The steel slag used in this paper has undergone metal iron separation and a pre-treatment with “hot steaming”. Besides, to improve environmental performance, the high performance concrete is mainly made of recycled IOTs. In the end, the author verifies the mechanism of the improved performance so that the findings can benefit the future research in this area.

2. MATERIALS AND METHODS

2.1 Raw materials

The converter steel slag used in this study are provided by Ansteel, Liaoning, China. See Table 1 for the results of chemical composition analysis of the steel slag. The f-CaO content is as low as 0.82%, much lower than the allowable content in Portland cement clinker specified by the Chinese national standard (GB/T 21372-2008). The ignition loss reaches 5.04%, indicating that the steel slag has been hydrated during the “hot steaming” pretreatment. Most of the metal iron particles have been separated away, and the identifiable crystallized phases in the steel slag include β-belite, γ- belite, alite, $Ca(OH)_2$ and RO phases [12].

Gathered from Qidashan IOTs impoundment of Ansteel, the IOTs in this study are generated during the froth flotation of iron ore concentrates. The IOTs are among the finest in the world. The particles are mostly between 0.63mm and 0.043mm. Less than 1% of the particles are larger than 0.63mm and about 10.43% of them are smaller than 0.043mm. See Table 1 for the results of chemical composition analysis of the IOTs. As shown in the table, the SiO_2 content of the IOTs sample is 72.12%, which is resulted from the high silica content. X-ray Diffraction (XRD) analysis suggests that the most important mineral in the IOTs is quartz. There are also traces of hematite, chlorite, and amphiboles [12].

Other raw materials include granulated blast furnace Slag (GBFS) from Shougang Group, Portland cement clinker from Tangshan Jidong Cement Co. Ltd., and flue gas desulfurization gypsum (GFGD) provided from Shijingshan Power Plant in Beijing. The chemical composition of all these raw materials is also shown in Table 1.

Table 1. Chemical composition of raw materials (%)

Composition	Steel slag	IOTs	GBFS	Cement clinker	GFGD
SiO_2	12.22	72.12	32.70	22.50	3.16
Al_2O_3	6.84	3.04	15.40	4.86	1.35
Fe_2O_3	14.53	12.62	0.40	3.43	0.47
FeO	11.83	3.44	-	0.02	0.086
MgO	11.00	1.13	8.97	0.83	7.49
CaO	35.82	2.96	38.79	66.30	33.38
f- CaO	0.82	-	-	-	-
MnO	1.54	0.17	0.02	-	0
SO_3	0.42	0.16	1.93	0.31	45.70
Loss	5.04	3.06	0.76	0.96	8.28

2.2 Preparation of cementitious material

After the removal of metal iron particles, the steel slag is milled for 90min. The resulting steel slag power is processed to reach the Blain fineness of 624m^2/kg. See Figure 1 for the particle size distribution of the milled steel slag powders. Other raw materials are milled and mixed by the “step-milling” method, creating a mixture of IOTs, GBFS, cement clinker, and GFGD (hereinafter referred to as IGCG). In the IGCG mixture, the ratio of IOTs: GBFS: cement clinker: GFGD is 20:26:26:8 by weight. The “step-milling” is carried out in the following procedures. Firstly, the IOTs are milled to reach 316m^2/kg in Blain fineness; secondly, the milled IOTs are mixed with the original GBFS and the mixture is further milled to reach 494m^2/kg in Blain fineness; thirdly, the milled mixture of IOTs and GBFS is mixed with original GFGD and cement clinker, which has been pre-crushed to smaller than 10mm in grain size; fourthly, the mixed material containing IOTs, GBFS, GFCD and cement clinker is milled again to reach 607m^2/kg in Blain fineness, thus obtaining the IGCG mixture. See Figure 1 for the particle size distribution of the IGCG mixture. Next, the IGCG mixture is mixed with steel slag powder by the weight ratio of 4:1 to form the cementitious material SIGCG. All of the milling operations are carried out in a standard 5kg laboratory mill at a standard

media charge ratio pre-set by the mill manufacturer. For all milling operations, Material to be milled is kept constant at 5kg.

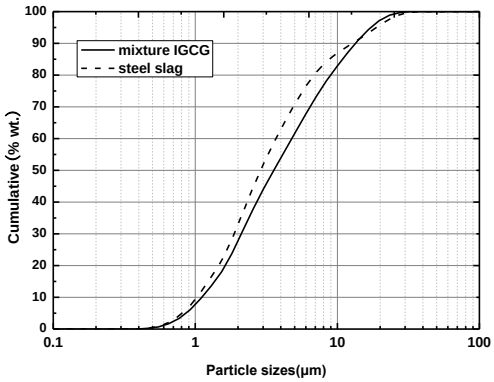

Figure 1. The particle size distribution ofthe IGCG mixture and the steel slag powder

2.3 Experimental methods

To prepare concrete samples, the original IOTs are used as fine aggregates, and no coarse aggregate is used. The author cements the original IOTs with the prepared SIGCG to create concrete specimens, and put the concrete specimens into one group, known as Group TS. For the specimens in Group TS, the weight ratio between the original IOTs and the cementitious material is 1:1, and the ratio between water and the cementitious material is maintained a constant value of 0.23. Added as the chemical admixture, the polycarboxylate superplasticizer is 0.4% by weight relative to the cementitious material SIGCG.

In accordance with the Chinese national standard (GB/T 50082-2009), the author prepares 100×100×515mm specimens and carries out autogenous shrinkage tests on them. The concrete mixtures are casted into 100×100×515mm molds. To ensure accurate measurement by the dilatometer, brass bolts are added to the two ends. Three replicates are fabricated for each mixture. After the casting, the specimens are covered with polyethylene films and kept in an artificial climate room during the setting period. Immediately after demolding (24 hours after mixing), all specimens receive an initial length measurement. Next, the specimens are cured in a warm curing room at 56°C and 100% relative humidity for 12 hours. Finally, the specimens are put in storage in a standard curing room at 20±1°C and 90% relative humidity. At every pre-set curing stage, namely 1day, 3 days, 7 days, and 28 days, the specimens are taken out for length measurement, and put back into the standard curing room immediately after the measurement until they are taken out again for the next measurement. For the purpose of comparing the autogenous shrinkage behavior between the concrete proposed in this paper and the common concrete of railway sleepers, the author also processes common concrete of railway sleepers into specimens of the same size above. The curing condition (100% relative humidity, 56°C, 12 hours) simulates the actual production condition in railway sleeper factories.

In accordance with the Chinese national standard (GB/T 1761-1999), strength tests are performed on 40×40×160mm specimens, which are prepared and cured in the same conditions with those of shrinkage test specimens. Both bending strength and compressive strength are tested at 3 days, 7 days and 28 days during the curing process.

To simply the analytical process, only neat SIGCG cementitious material is used to prepare the specimens. The original IOTs aggregates are not used because of their poor hydrability. Apart from that, the original IOTs aggregates are extracted from the analytical specimens, and mixed and cured in the same conditions with those of the shrinkage test and strength test specimens.

The author uses the following instruments. The XRD analysis is conducted with Cu Kα radiation on a Rigaku D/max 2550 spectrometer. The working voltage is 50kV. The IR was performed on a Fourier transform infrared spectrometer (NEXUS-70). The morphology and microstructure of the specimens are observed on a Zeiss SUPRATM55. Involving thermogravimetric (TG) investigation and differential scanning calorimetry (DSC), the thermal analysis is carried out on a Netzsch STA 449C. Data collection is conducted at atmospheric pressure, with the temperature increasing by 10°C /min to 1000°C.

3. RESULTS

3.1 Strength and autogenous shrinkage

The concrete specimens made of SIGCG and original IOTs aggregates are put into one group, known as Group TS. See Table 2 for the bending and compressive strength of the concrete specimens. As shown in the Table, the compressive strength exceeds 80MPa after 28 days of curing. This satisfies the requirement for most high-strength concretes used in engineering structure. Besides, the bending strength of the concrete is very high, nearly twice of that of common C80 concrete. Figure 2 also compares the autogenous shrinkage between the IOTs-based concrete specimens and the specimens of the common concrete for railway sleepers. As shown in the figure, Group TS concrete has a much smaller autogenous shrinkage than that of the common concrete for railway sleepers, especially at the curing age of 7 days and 28 days. For example, Group TS concrete specimens have an average autogenous shrinkage of 77μm/m at 7 days, while the specimens of the common concrete for railway sleepers have an average autogenous shrinkage of 304μm/m under the same curing condition. At the curing age of 28 days, the average autogenous shrinkage of Group TS concrete specimens and the specimens of the common concrete for railway sleepers are respectively 194μm/m and 464μm/m.

As suggested by the above test results, the steel slag powder can significantly reduce the autogenous shrinkage of IOTs-based concrete. Thus, the stress loss could be greatly reduced if the concrete is applied to the prestressed reinforcement in prefabricated structures.

Table 2. The strength of Group TS concrete specimens

Group TS	3 days	7 days	28 days
Bending strength (MPa)	15.08	16.23	17.63
Compressive strength (MPa)	56.10	73.66	86.36

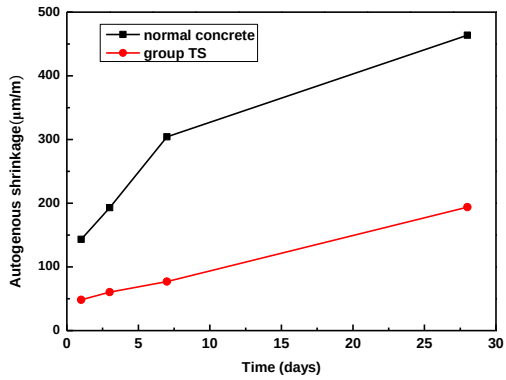

Figure 2. Comparison of autogenous shrinkage between IOTs-based concrete specimens of Group TS and the common concrete specimens

3.2 Phase evolution, micro-morphology and micro-texture

3.2.1 XRD analysis

Figure 3 displays the XRD patterns of specimens made from neat SIGCG without adding any aggregates and cured for 3 days, 7 days and 28 days, respectively. The author analyzes the compositions on the basis of a database and some previous studies that have provided the structure of compounds and their corresponding peaks in cement [14-15]. As shown in Figure 3, in all of the three specimens, the major crystalline phases detected by XRD analysis are quartz, ettringite, portlandite and RO phase. To be specific, quartz comes from by IOTs, and RO phase from the steel slag. Portlandite may come from the steel slag and the hydration of clinker and steel slag. Ettringite is the only detectable crystallized phase that is newly formed during the hydration process. Moreover, C_2S, C_3S, C_3A, C_4AF, gypsum, C_2F, f-CaO, and f-MgO are definitely contained in cement clinker and GFGD, and can be clearly detected in the XRD spectrogram of steel slag. However, they are not detected in any of the specimens after 3 days, 7 days and 28 days. Other crystallized phases in IOTs, such as chlorite, hematite and amphiboles, are also not detected in these specimens. Brought in by the raw materials, these crystallized phases could not be detected in the XRD patterns of specimens cured for 3 days, 7 days and 28 days. The main reason goes as follows: During the mixing process to product the SIGCG, the percentage of these crystallized phases are greatly lowered from the levels in individual raw material. The other reason is that some of these crystallized phases originally introduced to the specimens are largely consumed or totally diminished by hydration in the curing process. Hydration might also be the cause of micro-expansion and reduction in the autogenous shrinkage. As the products of the hydration of f-CaO and f-MgO, $Ca(OH)_2$ and $Mg(OH)_2$ lead to an increase in solid volume by 98% and 148%, respectively [16-19]. According to Figure 1, the milled steel slag powders fall between 0.8μm and 80μm in particle size, of which 50% are smaller than 2.92μm, 40% are smaller than 12.83μm. Consequently, the very fine particles hydrates faster than coarser particles. Furthermore, in the form of lime and periclase, the f-CaO and f-MgO are highly crystallized and thereby not very active in hydration. Thus, the hydration of f-CaO and f-MgO during concrete curing is bound to be a continuous, time-consuming process, which reduces the autogenous shrinkage in the long run [20].

Traditionally recognized as an inert phase during hydration [21], RO phase has a high content of steel slag. However, it is inevitable for very fine particles of RO phase, such as the sub-micron particles, and the surfaces of coarser particles to react with water, particularly when the RO phase are is rich in MgO. The hydration of very fine particles and the surfaces of coarser particles is expected to form $Mg(OH)_2$ and other hydrated phases, and cause micro-expansion during the curing of the specimens.

Two other prominent characters are clearly recognizable from the XRD spectrogram in Figure 3. First, the spectra of 3 days, 7 days and 28 days all exhibit the same curve pattern between 20° and 40°. The curve is increasingly prominent as the curing time extends from 3 days to 28 days. This suggests that the specimens have a large quantity of non-crystallized phases or very low crystallized phases and the quantity increases continuously during the curing process. As shown in Table 2, the compressive strength of the 28 day curing specimens surpasses that of the 3 day curing specimens by more than 30%, signifying the continuous formation of C-S-H and other cementitious hydration products during the curing process. Another noticeable change in the XRD spectrogram lies in the protlandite peak, which becomes slightly higher as the curing time extends from 3 days to 28 days. This suggests that the $Ca(OH)_2$ concentration or crystallinity increases in the curing process. The $Ca(OH)_2$ produced by the hydration of cement clinker and steel slag in the early stage could be consumed quickly by the pozzolanic reaction of very fine GBFS and IOTs. Figure 1 clearly depicts that nearly 10% of the particles of SIGCG are submicron-sized. Besides, the submicron particles are mostly IOTs grains and some are nanometer-sized [22]. The phenomenon reflects the effect of the “step-milling” of IOTs, which are milled for a longer time than any other raw material. The pozzolanic reactions of these submicron-sized and nanometer-sized IOTs are very likely to happen in the early stage of curing and subsequently consume $Ca(OH)_2$ in a timely manner. With the passage of curing time, very fine IOTs and GBFS are quickly consumed in pozzolanic reactions, and the total pozzolanic reaction speed in the system gradually slows down, which in turn results in a drop in the consumption rate of $Ca(OH)_2$. When the consumption rate falls below the $Ca(OH)_2$ formation via the hydration of residue clinker and steel slag, the total amount of free $Ca(OH)_2$ would increase. In addition, longer curing time also allows $Ca(OH)_2$ crystals to grow in size and crystallinity, making the peaks of $Ca(OH)_2$ grow higher in the spectogram with the increase in curing time. Take the peak of portlandite at 60° as an example, the peaks of 3 days and 7 days are similar in height, but the peak of 28 days is significantly taller. In terms of peak intensity, the ration between 3 days and 28 days is about 2.5:4. The pattern echoes with previous research findings that the $Ca(OH)_2$ produced by cement hydration early on has very fine grain size and very low crystallinity, but both parameters increase as the hydration time grows [23].

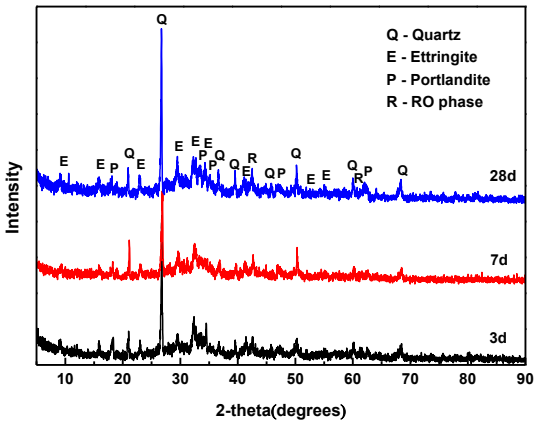

Figure 3. XRD spectrogram of hydrated neat SIGCG specimens

3.2.2 IR analysis

Figure 4 shows the IR spectra of hydrated neat SIGCG specimens cured for different times. As shown in the figure, the absorption bands around 459cm^{-1} and 795cm^{-1} correspond to the bending vibration of Si-O-Si bond and the stretching vibration of Si-O-Si bond in quartz, respectively. As the curing time increases, there is a clear decrease of transmittance of these two bands. This suggests that the total amount of quartz decreases during the curing process. It is further concluded that some very fine quartz grain particles produced by the "step-milling" participate the pozzolanic reaction during the curing process. The conclusion is in good agreement with the results of the XRD analysis.

The absorption band around 990cm^{-1} reflects the asymmetric stretching vibration of Si-O-Si bond in C-S-H gels [24], which indicates there is plenty of short chains of hydrated silica tetrahedrons. What is more, the absorption band becomes stronger during the curing process, revealing a continuous growth in the total amount of C-S-H gels. The absorption band around 1645 cm^{-1} reflects the bending vibration of O-H bond of hydroxyl water or crystallized water, and the band around 3425cm^{-1} reflects the O-H stretching vibration of hydroxyl crystallized water in C-S-H gels [25]. It is clearly illustrated in Figure 4 that these two bands also become stronger in all specimens of 3 days, 7 days and 28 days of curing. This again reveals the continuous growth of the amount of C-S-H in the specimens during the curing process.

The formation of ettringite is manifested by two absorption bands around 3635cm^{-1} and 1090cm^{-1}. The absorption band around 1090cm^{-1} reflects the asymmetric stretching vibration of S-O bond typically in ettringite [25]. As shown in Figure 4, the absorption band around 1090cm^{-1} is slightly sharper and stronger with the increase in curing time, indicating that the ettringite mineral becomes slightly higher in crystallinity and larger in quantity as the curing time lengthens. The result coincides with the XRD analysis in the preceding section. The absorption band around 3635cm^{-1} reflects the stretching vibration of H-O-H bond in crystallized water of ettringite. This and is not very prominent and is mostly overlapped by the band around 3245cm^{-1} which reflects the hydroxyl water of C-S-H gels. O-H bond is not typically strong in C-S-H gels because the latter features low crystallinity and complex micro-texture. Some O-H bonds are affected by the hydrogen bonds between water molecules in the solution as well as other factors. Thus, the bonding energy of O-H in C-S-H gels varies in a wide range. Sometimes, it even overlaps that of crystallized water. Nevertheless, crystallized water is not the only form of water in ettringite. Some water exist in the form of hydroxyl. The O-H bond of crystallized water differs in bonding energy from that of hydroxyl water in ettringite crystals. The multifold overlap of O-H bonding energy in C-S-H gels and ettringite is demonstrated by the wide and strong absorption band between 3000cm^{-1} and 3750cm^{-1}. Within this range, there are two absorption peaks, the taller appears at 3425cm^{-1} and the shorter at 3635cm^{-1}.

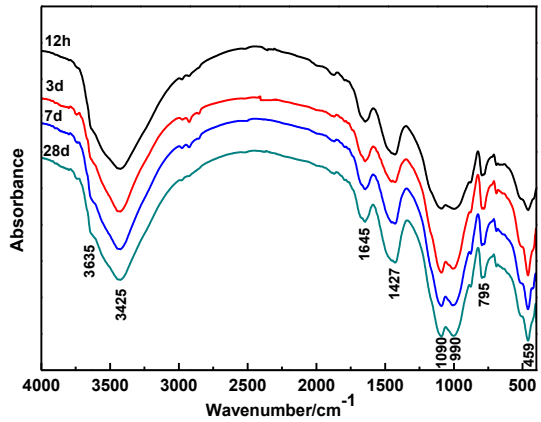

Figure 4. IR spectra of hydrated neat SIGCG specimens

3.2.3 DSC-TG analysis

Figure 5 shows the DSC-TG curves of hydrated neat SIGCG specimens cured for different ages from 12 hours, 3 days, 7 days to 28 days. As shown in Figure 5(a), five endothermic peaks are recognizable. The peak values are T_{max}=117.5°C, T_{max}=143.3°C, T_{max}=445.4°C, T_{max}=697.8°C and T_{max}=808.5°C on the DSC curve of specimen cured for 12 hours. Based on thermogravimetric analysis, Göril Möschner [26] points out that ettringite phases lose their water molecules between 30°C and 150°C. As a result, the exothermal peak at T_{max}=117.5 °C is mainly caused by the dehydration of ettringite, accompanied by the dehydration of C-S-H gels and gypsum. The exothermal peak at T_{max}=143.3°C is caused by the dehydration of gypsum semihydrates [27]. The exothermal peak at T_{max}=445.4 °C is caused by the dehydration of $Ca(OH)_2$, probably accompanied by the dehydration of $Mg(OH)_2$ [28]. The exothermal peak at T_{max}=697.8°C is caused by the decomposition of newly formed low crystalline $CaCO_3$, probably accompanied by the decomposition of well crystallized iron-rich dolomite [29], which is generated by the long-lasting carbonation of steel slag during "hot steaming" and storage. This endothermic peak might also be attributable to a possible phase change from β-C_2S to α-C_2S [30]. The exothermal peak at T_{max}=808.5 °C is caused by the decomposition of well crystallized calcite [29], probably accompanied by the final dehydration of C-S-H, involving minerals like xonotlite [31]. The exothermal peak at T_{max}=863.0°C is caused by the crystallization of wollastonite from the dehydrated C-S-H. Actually, this peak appears as a non-prominent concave curve consisting of numerous tiny peaks in the temperature range between 840°C and 920°C, suggesting that the structure of dehydrated C-S-H is not well organized before the crystallization of wollastonite. The TG curve in Figure 5(a) can be divided into three zones. Zone one is between 50°C and 400°C. It corresponds to the largest

endothermal peak on the DSC curve, which is caused by the dehydration of ettringite, C-S-H and gypsum. The total weight loss in zone one is 5.33%. Zone two lies between 400°C and 750°C, which covers the dehydration of $Ca(OH)_2$ and $Mg(OH)_2$, de-carbonation of newly formed low crystalline calcite, and probably well crystallized iron-rich dolomite. The total weight loss in zone two is 2.57%. Zone three falls between 750°C and 1,000°C, which covers the de-carbonation of well crystallized calcite [29], and probably the final dehydration of C-S-H, involving minerals like xonotlite. The total weight loss in zone three is 1.01%.

Four endothermic peaks are identified in Figure 5(b) on the DSC curve of the specimens cured for 3 days. The peak values are T_{max}=115.3°C, T_{max}=446.9°C, T_{max}=695.5°C and T_{max}=806.7°C, respectively. Among the four endothermic peaks, only the peak at T_{max}=115.3°C is prominent, while the other three small peaks appear as non-prominent convex curves consisting of numerous tiny peaks within a small range. With lightly lower temperature than the comparable peak (T_{max}=117.5°C) in Figure 5, the peak at T_{max}=115.3°C is probably affected by the fact that the ettringite becomes richer in iron and CO_3^{2-} due to the hydration of RO phases or other iron-rich phases of the steel slag. Besides, some ultra-fine particles of $Ca(OH)_2$, $Mg(OH)_2$, calcite and dolomite could have been consumed by the continuous formation of ettringite and C-S-H gel [32]. This is reflected by the TG curve in Figure 5(b), on which the total weight loss between 400°C and 1000°C is 1.5% more than that in Figure 5. The absence of peak T_{max}=143.3°C in Figure 5(b) indicates that gypsum is almost fully consumed from 12 hours to 3 days. This agrees well with the XRD analysis, in which no gypsum peaks are detected in the specimens cured for 3 days, 7 days, and 28 days. It is obvious that gypsum is mainly consumed during the formation of ettringite because among all of the newly formed mineral groups in the specimens cured for 3 days, 7 days, and 28 days, ettringite mineral is the only one identified as SO_4^{2-} rich. The endothermic peak at T_{max}=882.5 °C is caused by the crystallization of wollastonite in dehydrated C-S-H. This peak is much sharper and deeper than the comparable concave curve peak (T_{max}=863.0 °C) in Figure 5(a), suggesting that the amount of C-S-H gel has plunged and the structure of the dehydrated C-S-H is better organized before crystallization of wollastonite than that of the 12h specimens.

Both Figure 5(c) and Figure 5(d) have similar curve patterns with Figure 5(b) but all the peaks become sharper and sharper from Figure 5(b) to Figure 5(c) and to Figure 5(d). This proves that, as the curing time increases from 3 days to 28 days, quantity increase and structure improvement has happened to most hydrated phases and carbonate phases. The TG curves of Figures 5(b), 5(c) & 5(d) exhibit a continuous increase on total weight loss from 8.35%, 9.66% to 12.04% within the temperature range between 50°C and 1,000°C. When it comes to the temperature range between 50°C and 400°C, which is the most important temperature range for the dehydration of C-S-H gel and ettringite minerals, the accumulated weight losses are 6.23%, 7.33% and 8.49% for the samples cured for 3 days, 7 days, and 21 days, respectively. This not only agrees well with the strength development of the specimens, but also complies with the results of XRD and FIR analysis.

Another noticeable trend in Figures 5(b), 5(c) & 5(d) is that the two peaks at about T_{max}=375.1°C and T_{max}=458.0°C become increasingly prominent. The two peaks are caused by the dehydration of $Mg(OH)_2$ and $Ca(OH)_2$ [28]. The trend reflects the increasing accumulation of $Mg(OH)_2$ and $Ca(OH)_2$ in the specimens with the increase in curing time, and gives direct evidence for the continuous hydration of MgO bearing and CaO bearing phases, such as f-MgO, f-CaO, and probably RO phases. According to Figure 5(d), it is calculated that the mass loss on the DSC curve between 334°C and 416 °C reflects the dehydration of 1.42% $Mg(OH)_2$. The reaction is illustrated by the endothermic peak at 375.1°C. It is also learned that the mass loss on the DSC curves between416 °C and 477 °C reflects the dehydration of 3.86% $Ca(OH)_2$. The reaction is illustrated by the endothermic peak at 458.0 °C.

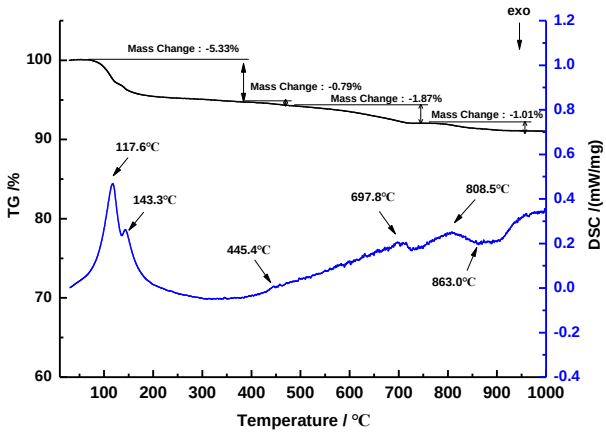

(a)

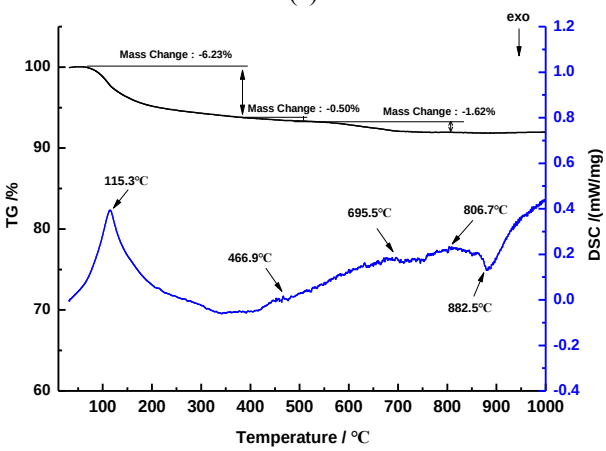

(b)

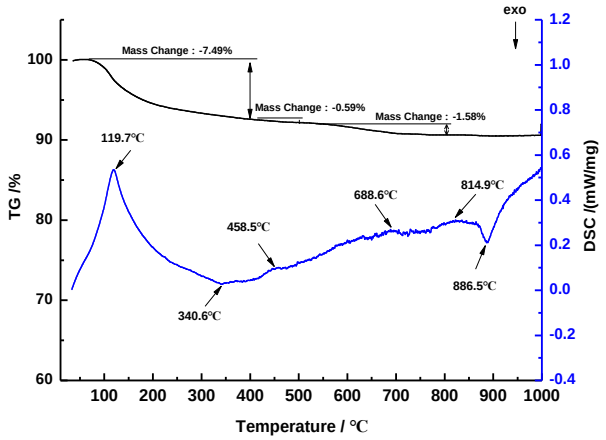

(c)

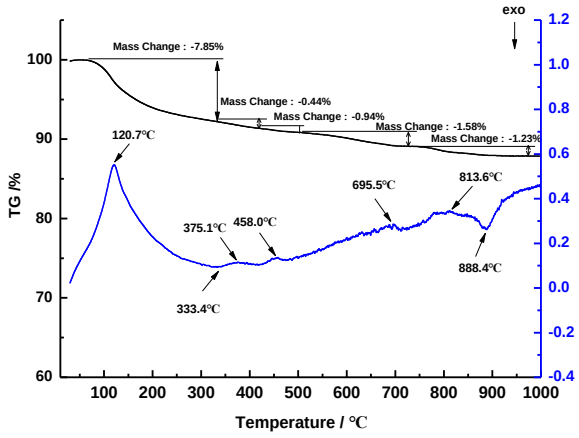

(d)

Figure 5. DSC -TG curves of hydrated neat SIGCG specimens cured for: a) 12 hours; b) 3 days; c) 7days; and d) 28days

3.2.3 SEM analysis

Figure 6 shows the SEM images of the broken surface of hydrated neat SIGCG cured for 3 days, 7 days and 28 days. As shown in the figure, both C-S-H gels and ettringite crystals are clearly recognizable in the specimens. Besides, there is an obvious trend of C-S-H growth in terms of quantity and compactness as the curing time lengthens, which is in good agreement with the results of XRD, IR and DSC-TG analysis. The figure also displays that there are still some unreacted coarser particles in all specimens, which contribute to the micro-aggregate effects in the concrete.

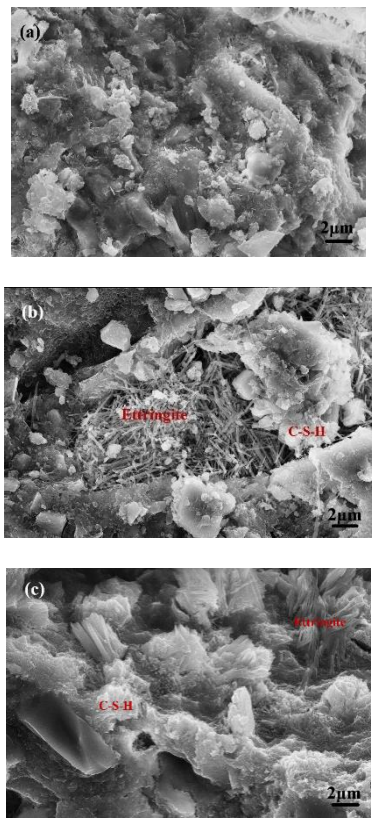

Figure 6. SEM images of the broken surface of the hydrated neat SIGCG specimens cured for: a)3 days; b) 7 days; and c) 28 days

3.3 Discussion

Giving overall consideration to the results of the strength tests, autogenous shrinkage tests, and the microscopic analysis, the author finds out that the cementitious material prepared by "step-milling" are characterized by high performance and low shrinkage. Containing 74% industrial wastes, the new cementitious material is more environmentally friendly and more sustainable compared to common Portland cement. The industrial wastes include IOTs, GBFS, steel slag and GFGD. Highly dispersed in the concrete, the very fine steel slag particles both reduce shrinkage and promote strength of the concrete. An apparent shrinkage reducing mechanism lies in the hydration of f-CaO, f-MgO and possibly MgO-rich RO phases. When $Ca(OH)_2$ is formed from crystallized oxide phases like f-CaO or crystallized calcia, the solid volume of the concrete would increase by 98% [18,19]. When $Mg(OH)_2$ is formed from crystallized oxide phases like f-MgO or crystallized periclase, the solid volume of the concrete would increase by 148% [18,19]. This shrinkage reducing mechanism is depicted by DSC-TG analysis as $Ca(OH)_2$ and $Mg(OH)_2$ accumulation is exhibited by specimens cured from 3 days to 28 days. The strength enhancement effect of the very fine steel slag particles is caused by two reasons. First, these particles contain β-belite, γ- belite, and alite [15], and most of them are micron-sized or even submicron-sized. The particles are easily hydrated to form C-S-H gels and $Ca(OH)_2$. Second, the very fine steel slag particles contain $Ca(OH)_2$ generated in the "hot steaming" pretreatment. Coupled with the newly formed $Ca(OH)_2$, the particles make a significant contribution to the ettringite formation and pozzolanic reaction of GBFS and sub-micron sized IOTs.

During the curing process, particularly in the first 3 days, there is an apparent coordinated growth between C-S-H gel and ettringite, which is also capable of reducing shrinkage and promoting strength of the concrete. If the system is completely open to and saturated with free water in the environment, the solid phase volume would increase substantially during the formation of ettringite because a lot of water is crystallized in the process [34]. However, the concrete curing system proposed in this paper is neither completely open to and saturated with, nor completely closed to the free water in the environment. Instead, the specimens are cured in an environment of 20°C and 90% relativity humidity, and prepared with a very low ratio between water and the cementitious material, which inevitably causes self-desiccation. Therefore, it is impossible to make accurate estimation of the micro-expansion resulted from the formation of ettringite. Much research is yet to be done to properly estimate the effect. It should be noted that weight ratio of clinker to GFGD is 26:8 in this system, much smaller than that of common Portland cement, which is 80:5 as specified by the Chinese national standard GB 175-2007. The clinker in this system can only provide 1.3% Al_2O_3 to the cementitious material, which is far from enough to consume all of the gypsum needed to form ettringite. Nonetheless, the DSC-TG analysis suggests that nearly all of the gypsum has been consumed after 3 days of curing. This leads to another question: how is alumina is attracted from other raw materials to form the ettringite? The fact is, the cementitious material in this paper contains a high content of GBFS, and has been milled to particles much finer than common GBFS powders used in concrete. As a result, the GBFS powders

used in this study is much more active than common ones during hydration. Besides, the GBFS is mainly composed of silicate glasses, inw which nearly all of the Al^{3+} are tetrahedrally coordinated by oxygen [35]. Alumina tetrahedrons and silica tetrahedrons are connected together disorderly to form glassy networks. Cations like Ca^{2+} and Mg^{2+} distribute around the alumina tetrahedrons to balance the shortage of the positive charges in the alumina tetrahedrons. When the surface of very fine GBFS particles is exposed to concrete fluid featuring a high OH^- concentration, the cations like Ca^{2+} and Mg^{2+}onthe surface dissolve into the solution rapidly. The dissolution intensifies the electrical charge imbalance, which in turn promotes the disjointing of alumina tetrahedrons from the alumina-silicate glassy networks.

The dissolved alumina tetrahedrons are most likely to exist in the forms of $H_3AlO_4^{2-}$, $H_2AlO_4^{3-}$, $H_2AlO_3^-$, $HAlO_3^{3-}$, AlO_2^-, as well as other similar species, and tend to reach the solubility equilibrium with GBFS particle surfaces. If there are free gypsum particles in the system, ettringite is rapidly formed by the reaction shown in equation (1).

$$4H_3AlO_4{}^{2-} + 6Ca^{2+} + 6CaSO_4 \cdot 2H_2O + 4OH^- + 44H_2O \rightarrow 2(3CaO \cdot Al_2O_3 \cdot 3CaSO_4 \cdot 32H_2O) \quad (1)$$

With solubility product constant of $10^{-111.6}$, ettringite has an extremely low solubility [36]. The continuous crystallization of ettringite consumes $H_3AlO_4^{2-}$ or other similar species quickly, and breaks the solubility equilibrium between the GBFS particle surface and $H_3AlO_4^{2-}$ or other similar species. Subsequently, more aluminate trahedrons are dissolved. The disjointing effect greatly improves the activity of remaining clusters of silicate trahedrons on GBFS particle surfaces. The resulting active small clusters of silica-alumina tetrahedrons generate complicated C-S-H gels by reacting with cations like Ca^{2+} and Mg^{2+}. As the disjointed small clusters of silica-alumina tetrahedrons migrate away from GBFS particle surfaces, new surfaces are continuously exposed to the solution. A new cycle of dissolution (Ca^{2+}, Mg^{2+}, $H_3AlO_4^{2-}$ and similar species) and formation (ettringite) ensues, forming more and more complicated C-S-H gels. Although the formation of C-S-H gels induces the autogenous shrinkages of concrete, the effect can be counterbalanced by the unapparent expansion caused by crystallization of ettringite during the curing process, provided that sufficient curing water are in place. The coordinated effect of C-S-H gels formation and ettringite crystallization both promotes concrete strength and reduces autogenous shrinkage.

It worth mentioning that in the SIGCG concrete, the weight ratio of IOTs can be as high as 60% and that of industrial wastes can be as high as 87%. Using original fine grain IOTs as aggregates without any normal sands or gravels, the concrete boasts a much smaller autogenous shrinkage than that of common concrete for railway sleepers. Therefore, the proposed concrete can overcome the obstacles of autogenous shrinkage of IOTs-based concrete and has a great potential to serve as the material for prefabricated structures or cast-in-situ concretes.

4. CONCLUSION

In this paper, the author prepares a low-shrinkage, high-strength concrete by using original fine grain IOTs as aggregates, and a step-milled mixture of IOTs, GBFS, cement clinker, GFGD, and steel slag powder as the cementitious material. From strength tests, XRD, FTIR to SEM, a series of tests are conducted to evaluate the performance of the proposed concrete and to uncover the mechanisms beyond the observations. Based on the test results and discussion above, the author draws the following conclusions:

1)According to shrinkage measurement and strength tests, the proposed concrete has a much lower autogenous shrinkage and much higher strength than ordinary concretes.

2) According to the XRD analysis, the prominent decrease of autogenous shrinkage is mainly attributable to the micro-expansion caused by the hydration of f-CaO, f-MgO and part of the very fine particles of RO phases.

3)According to IR, DSC-TG and SEM analysis, there is a clear increase of ettringite and C-S-H gels concentration during the curing of the proposed concrete.

4) The proposed IOTs-based concrete has a great potential to serve as the material for prefabricated structures or cast-in-situ concretes.

ACKNOWLEDGMENT

The authors would like to thank the support from the National Hi-Tech Research and Development Program of China (863 program) (2012AA062405) and Natural Science Foundation of China (NSFC) (41472043).

REFERENCES

[1] J. Sun, Z. A. Jiang, W. Ni, “Real-time simulation of soot behavior generated by blasting,” *Blasting*, vol. 23, no. 1, pp. 1-5, Mar., 2006.

[2] National Development and Reform Commission, China, “Annual report on resources comprehensive utilization,” 2014, 7-10.

[3] S. Yang, F.D. Liu, Y. Li, Z. Hui, et al., “Production of lightweight ceramisite from iron ore tailings and its performance investigation in a biological aerated filter (BAF) reactor,” *J. Hazard. Mater*., vol. 178, no. 1-3, pp. 999-1006, June, 2010. DOI: 10.1016/j.jhazmat.2010.02.038.

[4] Alberto Mirandola and Enrico Lorenzini, “Energy, environment and climate: From the past to the future,” *International Journal of Heat and Technology*, vol. 34, no. 2, June, 2016, pp. 159-164, DOI: 10.18280/ijht.340201.

[5] Ines Boulaoued, Ines Amara and Abdallah Mhimid, “Experimental determination of thermal conductivity and diffusivity of new building insulating materials,” *International Journal of Heat and Technology*, vol. 34, no. 2, June, 2016, pp. 325-331. DOI: 10.18280/ijht.340224.

[6] Y.C. Zheng, W. Ni, L. Xu, et al., “Mechanochemical activation of iron ore tailings and preparation of high-strength construction materials,” *J. Univ. Sci. Technol*. B., vol. 32, no. 4, pp. 504-508, Apr., 2010.

[7] P. Lura, K. van Breugel, I. Maruyama, "Effect of curing temperature and type of cement on early-age shrinkage of high-performance concrete," *Cem. Concr. Res*., vol. 31, no. 12, pp. 1867-1872, Dec., 2001. DOI: 10.1016/S0008-8846(01)00601-9.

[8] M.H. Zhang, C.T. Tam, M.P. Leow, "Effect of water-to-cementitious materials ratio and silica fume on the autogenous shrinkage of concrete," *Cem. Concr. Res*., vol. 33, no. 10, pp. 1687-1694, Oct., 2003. DOI: 10.1016/S0008-8846(03)00149-2.

[9] S.I. Igarashi, A. Bentur, K. Kovler, "Autogenous shrinkage and induced restraining stresses in high-strength concretes," *Cem. Concr. Res*., vol. 30, no. 11, pp. 1701-1707, Nov., 2000. DOI: 10.1016/S0008-8846(00)00399-9.

[10] E. Lepage, M. Balbaki, E. Dallalre, et al., "Early shrinkage development in a high performance concrete," *Cement. Concrete. Aggr., vol.* 21, no. 1, pp. 31-35, June, 1999. DOI: 10.1520/CCA10505J

[11] Q. Wang, P.Y. Yan, "Hydration properties of basic oxygen furnace steel slag," *Constr. Build. Mater*., vol. 24, no. 7, pp. 1134-1140, July, 2010. DOI: 10.1016/j.conbuildmat.2009.12.028.

[12] H. Wu, W. Ni, X. W. Cui, et al., "Preparation of concrete sleeper using hot steaming steel slag with low autogenous shrinkage," *Transactions of Materials and Heat Treatment*., vol. 35, no. 4, pp. 7-12, Apr., 2014.

[13] Y. Huang, G.P. Xu, H.G. Cheng, et al., "An overview of utilization of steel slag," *Proc. Environ. Sci*., vol. 16, pp. 791-801, Dec., 2012. DOI: 10.1016/j.proenv.2012.10.108.

[14] Stepkowska, E. T., M. A. Aviles, J. M. Blanes and J. L. Perez-Rodriguez, "Gradual transformation of $Ca(OH)_2$ into $CaCO_3$ on cement hydration," *Journal of Thermal Analysis and Calorimetry*, vol. 87, no. 1, pp. 189-198, Jan., 2007. DOI: 10.1007/s10973-006-7840-7.

[15] Qu, B., A. Martin, J. Y. Pastor, A. Palomo and A. Fernández-Jiménez, "Characterisation of pre-industrial hybrid cement and effect of pre-curing temperature," *Cement and Concrete Composites, vol.* 73, pp. 281-288, Oct., 2016. DOI: 10.1016/j.cemconcomp.2016.07.019.

[16] G. Wang, Y.H. Wang, Z.L. Gao, "Use of steel slag as a granular material: volume expansion prediction and usability criteria," *J. Hazard. Mater*., vol. 184, no. 1-3, pp. 555-560, Dec., 2010. DOI:10.1016/j.jhazmat.2010.08.071.

[17] H.N. Zhang, A.J. Xu, J. Cui, et al. "Overview and trend of steel slag recycling and reuse,"*Steelmaking*, vol. 28, no. 3, pp. 74-77, 2012.

[18] I.A. Altum, I. Yilmaz, "Study on steel furnace slags with high MgO as additive in Portland cement," *Cem. Concr. Res*., vol. 32, no. 8, pp. 1247-1249, Aug., 2002.

[19] S. Kourounis, S. Tsivilis, P.E. Tsakiridis, et al., "Properties and hydration of blended cements with steelmaking slag," *Cem. Concr. Res*., vol. 37, no. 6, pp. 815-822, June, 2007. DOI: 10.1016/j.cemconres.2007.03.008.

[20] T. Zhang, Q. Yu, J. Wei, et al. "Preparation of high performance blended cements and reclamation of iron concentrate from basic oxygen furnace steel slag," *Resour. Conserv. Recy*., vol. 56, no. 1, pp. 48-55, Nov., 2011. DOI: 10.1016/j.resconrec.2011.09.003.

[21] A.S. Abu-Eishaha, M.S.B. El-Diebb, "Performance of concrete mixtures made with electric arc furnace (EAF) steel slag aggregate produced in the Arabian Gulf Region," *Constr. Build. Mater*., vol. 34, no. 5, pp. 246-251, Sept., 2012.

[22] X.Y. Huang, W. Ni, L.P. Zhu, et al. "Grinding characteristic of Qidashan iron tailings," *J. Univ. Sci. Technol. B.*, vol. 32, no. 10, pp. 1253-1257, Oct., 2010.

[23] J. Stark, "Recent advances in the field of cement hydration and microstructure analysis," *Cem. Concr. Res.*, vol. 41, no. 7, pp. 666-678, July, 2011. DOI: 10.1016/j.cemconres.2011.03.028.

[24] R. Ylmén, U. Jäglid, B.M. Steenari, et al. "Early hydration and setting of Portland cement monitored by IR, SEM and Vicat techniques," *Cem. Concr. Res*., vol. 39, no. 5, pp. 433-439, May, 2009. DOI: 10.1016/j.cemconres.2009.01.017.

[25] T. Richard, L. Mercury, F. Poulet, et al., "Diffuse reflectance infrared Fourier transform spectroscopy as a tool to characterise water in adsorption/confinement situations," *J. Colloid. Interf. Sci.*, vol. 304, no. 1, pp. 125-136, Dec., 2006. DOI: 10.1016/j.jcis.2006.08.036.

[26] G. Möschner, B. Lothenbacha, F. Winnefeld, et al. "Solid solution between Al-ettringite and Fe-ettringite (Ca_6 $[Al_{1-x}Fe_x(OH)_6]_2(SO_4)_3$•$26H_2O$)," *Cem. Concr. Res*., vol. 39, no. 6, pp. 482-489, June, 2009. DOI: 10.1016/j.cemconres.2009.03.001.

[27] W. Sha, E. A. O'Neill, Z. Guo, et al. "Differential scanning calorimetry study of ordinary Portland cement," *Cem. Concr. Res*., vol. 29, no. 9, pp. 1487-1489, Sep., 1999. DOI: 10.1016/S0008-8846(99)00128-3.

[28] E. Nonnet, N. Lequeux, P. Boch, "Elastic properties of high alumina cement castables from room temperature to 1600°C," *J. Eur. Ceram.Soc*., vol. 19, no. 8, pp. 1575–1583, June, 1999. DOI: 10.1016/S0955-2219(98)00255-6.

[29] P.E. Grattan-Bellew, "Microstructural investigation of deteriorated Portland cement concretes," *Constr. Build. Mater*., vol. 10, no. 1, pp. 3–16, Feb., 1996. DOI: 10.1016/0950-0618(95)00066-6.

[30] N. R. Yang, W. H. Yue, "The handbook of inorganic nonmetallic materials atlas," Wuhan University of Technology Press, 2000.

[31] G.A. Khoury, "Compressive strength of concrete at high temperatures: a reassessment," *Mag. Concr. Res., vol.* 44, no. 161, pp. 291– 309, Jan., 1992. DOI: 10.1680/macr.1992.44.161.291.

[32] F. Guirado, S. Gali, J.S. Chinchon, "Thermal decomposition of hydrated alumina (CAH10)," Cem. Concr. Res., vol. 28, no. 3, pp. 381– 390, Mar., 1998. DOI: 10.1016/S0008-8846(98)00007-6.

[33] F. Wei, Y. N. Lv, X. H. Lan, et al., "Hydration products of fly ash cement-based material," *Journal of The Chinese Ceramic Society., vol.* 33, no. 1, pp. 52-56, Jan., 2005.

[34] Y. Li, J.L. Bao, Y.L. Guo, "The relationship between autogenous shrinkage and pore structure of cement paste with mineral admixture," *Constr. Build. Mater., vol.* 24, no. 10, pp. 1855-1860, Oct., 2010. DOI: 10.1016/j.conbuildmat.2010.04.018.

[35] L.P. Zhu, "Development of whole-tailings paste backfilling material using red mud and slag as the major components of cementing agent," *J. Univ. Sci. Technol. B*. 2012.

[36] C.B. Satish, Myneni, J. Samuel. Traina, Terry J. Logan, "Ettringite solubility and geochemistry of the $Ca(OH)_2$-$Al_2(SO_4)_3$-H_2O system at 1 atm pressure and 298 K," *Chemical Geology*, vol. 148, no. 1-2, pp. 1 – 19, June, 1998. DOI: 10.1016/S0009-2541(97)00128-9.